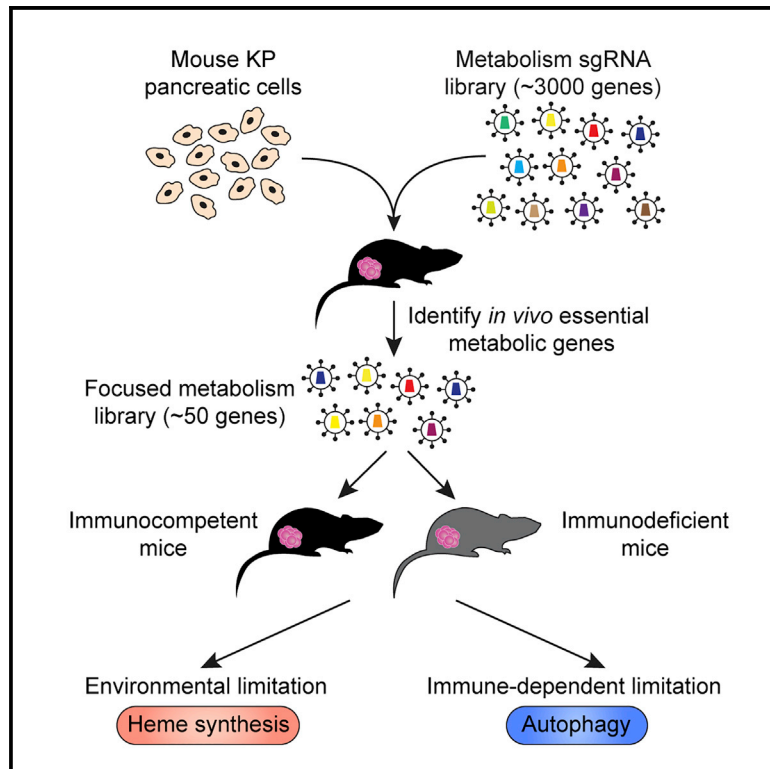


# Cell Metabolism

## Functional Genomics *In Vivo* Reveal Metabolic Dependencies of Pancreatic Cancer Cells

### Graphical Abstract



### Authors

Xiphias Ge Zhu, Aleksey Chudnovskiy, Lou Baudrier, ..., Gabriel D. Victora, Hani Goodarzi, Kıvanç Birsoy

### Correspondence

kbirsoy@rockefeller.edu

### In Brief

Using *in vivo* CRISPR screens, Zhu et al. map metabolic genes essential for pancreatic cancer cells to grow in culture and as tumors. While most essentialities are similar under these conditions, genetic screens identify heme synthesis and autophagy as metabolic requirements specific to the tumor environment.

### Highlights

- CRISPR screens identify metabolic genes essential for pancreatic tumor growth
- Most metabolic essentialities are similar in cells grown in culture and as tumors
- Heme synthesis is limiting due to increased heme degradation in the tumor environment
- Autophagy enables cancer cells to evade CD8+ T cell killing



## Resource

# Functional Genomics *In Vivo* Reveal Metabolic Dependencies of Pancreatic Cancer Cells

Xiphias Ge Zhu,<sup>1</sup> Aleksey Chudnovskiy,<sup>2</sup> Lou Baudrier,<sup>1</sup> Benjamin Prizer,<sup>1</sup> Yuyang Liu,<sup>1</sup> Benjamin N. Ostendorf,<sup>3</sup> Norihiro Yamaguchi,<sup>3</sup> Abolfozi Arab,<sup>4,5,6</sup> Bernardo Tavora,<sup>3</sup> Rebecca Timson,<sup>1</sup> Søren Heissel,<sup>7</sup> Elisa de Stanchina,<sup>8</sup> Henrik Molina,<sup>7</sup> Gabriel D. Victora,<sup>2</sup> Hani Goodarzi,<sup>4,5,6</sup> and Kıvanç Birsoy<sup>1,9,\*</sup>

<sup>1</sup>Laboratory of Metabolic Regulation and Genetics, The Rockefeller University, New York, NY, USA

<sup>2</sup>Laboratory of Lymphocyte Dynamics, The Rockefeller University, New York, NY, USA

<sup>3</sup>Laboratory of Systems Cancer Biology, The Rockefeller University, New York, NY, USA

<sup>4</sup>Department of Biochemistry & Biophysics, University of California, San Francisco, San Francisco, CA, USA

<sup>5</sup>Department of Urology, University of California, San Francisco, San Francisco, CA, USA

<sup>6</sup>Helen Diller Family Comprehensive Cancer Center, University of California, San Francisco, San Francisco, CA, USA

<sup>7</sup>The Proteomics Resource Center, The Rockefeller University, New York, NY, USA

<sup>8</sup>Antitumor Assessment Core Facility, Memorial Sloan Kettering Cancer Center, New York, NY, USA

<sup>9</sup>Lead Contact

\*Correspondence: [kbirsoy@rockefeller.edu](mailto:kbirsoy@rockefeller.edu)

<https://doi.org/10.1016/j.cmet.2020.10.017>

## SUMMARY

Pancreatic ductal adenocarcinoma (PDAC) cells require substantial metabolic rewiring to overcome nutrient limitations and immune surveillance. However, the metabolic pathways necessary for pancreatic tumor growth *in vivo* are poorly understood. To address this, we performed metabolism-focused CRISPR screens in PDAC cells grown in culture or engrafted in immunocompetent mice. While most metabolic gene essentialities are unexpectedly similar under these conditions, a small fraction of metabolic genes are differentially required for tumor progression. Among these, loss of heme synthesis reduces tumor growth due to a limiting role of heme *in vivo*, an effect independent of tissue origin or immune system. Our screens also identify autophagy as a metabolic requirement for pancreatic tumor immune evasion. Mechanistically, autophagy protects cancer cells from CD8+ T cell killing through TNF $\alpha$ -induced cell death *in vitro*. Altogether, this resource provides metabolic dependencies arising from microenvironmental limitations and the immune system, nominating potential anti-cancer targets.

## INTRODUCTION

Recent isotope labeling studies argue that the metabolism of human tumors is different from that of cancer cells in culture (Faubert et al., 2017; Hui et al., 2017). The tumor microenvironment in part drives this difference as cancer cells frequently starve for nutrients and oxygen due to dysfunctional vasculature. Indeed, changes in environmental nutrients and oxygen in culture can cause widespread effects on cancer cell metabolism (Alvarez et al., 2017; Birsoy et al., 2014; Cantor et al., 2017; Vande Voorde et al., 2019). Additionally, solid tumors are extraordinarily complex, containing diverse cell types including vascular cells, fibroblasts, and immune cells. Many non-cancerous cell types are in constant interaction with each other and provide metabolic support for growth and evasion of immune surveillance (Kishton et al., 2017). These observations raise the possibility that much of the work done in culture conditions may not reflect the cellular and nutrient complexities of human tumors. Despite recent attempts to recapitulate cancer metabolic states *in vivo* (Sullivan et al., 2019), nutrient composition of most human tumor types remains to be defined and the metabolic pathways that cancer

cells require to proliferate in the context of the stromal and immune cells remain poorly understood.

Pancreatic ductal adenocarcinoma (PDAC) is an aggressive disease characterized by a dense desmoplastic stroma, severe hypoxia, and an immunosuppressive microenvironment (Ryan et al., 2014). Mutations in *KRAS* and *TP53* are frequent in PDACs and contribute to metabolic changes that support anabolic processes as well as nutrient scavenging (Perera and Bardeesy, 2015). Previous work has identified metabolic pathways involved in PDAC progression such as autophagy, cysteine uptake, and alanine metabolism (Badgley et al., 2020; Sousa et al., 2016; Yang et al., 2018). However, we currently lack a complete understanding of essential metabolic pathways during pancreatic tumor progression or how environmental factors cause each of these dependencies. Such a study would identify potential therapeutic targets for these cancers with limited treatment options.

To address this, we performed genetic screens in a murine *Kras*<sup>G12D</sup>/*Trp53*<sup>R172H</sup> mutant (KP) PDAC cell line model using a metabolism-focused CRISPR library and compared metabolic dependencies of cancer cells grown in culture or as



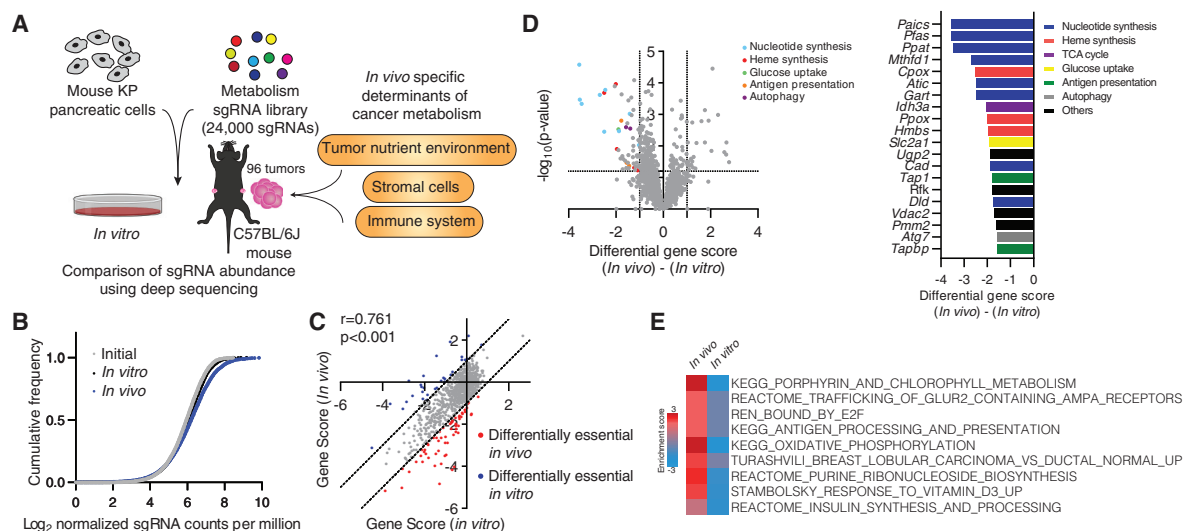


**Figure 1. Metabolism-Focused CRISPR Screens *In Vivo* Reveal Metabolic Dependencies of Pancreatic Tumors**

(A) Schematic of genetics screens to identify metabolic dependencies of KP pancreatic cancer specifically *in vivo*.

(B) Cumulative frequency curve of represented guides in genetic screens.

(C) Gene scores of *in vivo* versus *in vitro* genetic screens of KP pancreatic cancer growth.

(D) Volcano plot of differential gene scores comparing *in vivo* against *in vitro* conditions (left). Top 20 genes scoring as differentially required *in vivo*. Genes involved in specific metabolic pathways are indicated (right).

(E) Gene sets enriched in differentially required genes *in vivo* versus *in vitro* for pancreatic cancer growth. The heatmap generated by iPAGE represents the extent to which each gene set is enriched among the genes that are essential for tumor growth *in vivo*.

See also Figure S1.

tumors. These screens reveal a surprising similarity between essential metabolic genes for growth *in vitro* versus *in vivo*, suggesting that culture systems may be reasonable models for studying metabolic dependencies. Furthermore, we find several metabolic pathways as differentially required for tumor progression and determine selective pressures that may result in each metabolic dependency. Our analysis identifies heme synthesis as an *in vivo* liability due to environmentally induced upregulation of the heme-degrading enzyme Hmox1, an effect independent of the tissue origin or immune system. These screens also pinpoint autophagy as the only metabolic requirement for immune evasion. Loss of autophagy decreases tumor growth only in the presence of an intact immune system and enhances CD8+ T cell killing *in vitro*. Mechanistically, autophagy loss sensitizes pancreatic tumors to TNF $\alpha$ -induced apoptosis. Altogether, our work provides a comparative compendium of metabolic essentialities of pancreatic cancer cells grown in culture or as tumors, and reveals potential targets that could be exploited for therapy.

## RESULTS AND DISCUSSION

### Metabolism-Focused CRISPR Screens Reveal Essential Genes for Pancreatic Cancer Growth in Culture versus *In Vivo*

Pancreatic tumors rely on various cellular metabolic pathways to grow, but how nutrient environments modify these dependencies is not well understood. To begin to address potential differences in metabolic pathway dependencies of pancreatic cancer cells grown in tissue culture or as tumors, we con-

structed a metabolism-focused mouse sgRNA library targeting a comprehensive set of ~2,900 metabolic genes and performed parallel loss-of-function screens in a murine pancreas cancer cell line derived from a *Kras*<sup>G12D</sup>/*Trp53*<sup>R172H</sup> mutant (KP) PDAC mouse model (Figure 1A). This library contains sgRNAs targeting enzymes and small molecule transporters as previously reported (Birsoy et al., 2015), but also transcription factors and other regulators relevant to cellular metabolism. A full list of genes in the library is provided in Table S1. After transduction with the sgRNA library, we passaged the pool of knockout cells for 14 population doublings in culture but also formed subcutaneous tumors in an immunocompetent C57BL/6J mouse model. At the end of the screens, for each gene, we calculated its score as the median  $\log_2$  fold change in the abundance of all sgRNAs targeting the gene. Despite the challenge of maintaining sgRNA representation *in vivo*, we were able to detect an overwhelming majority (>99%) of sgRNAs from tumors, owing to the efficient engraftment of this syngeneic model (Table S1). Furthermore, indicating the robustness of the screening approach, cumulative sgRNA frequencies of cultured cancer cells showed only a slight enrichment in representation compared to those of tumors (Figure 1B). Gene sets related to metabolic processes such as glycolysis and glycosylation showed strong depletion (Figure S1A), consistent with the known essentiality of these pathways (Ohtsubo and Marth, 2006; Tsherniak et al., 2017; Xu et al., 2005). Notably, sgRNA abundances correlated remarkably well between tumors and cultured pancreatic cancer cells ( $r = 0.761$ ,  $p < 0.001$ ) (Figure 1C). These results suggest that, despite the nutritional and cellular differences between tumors

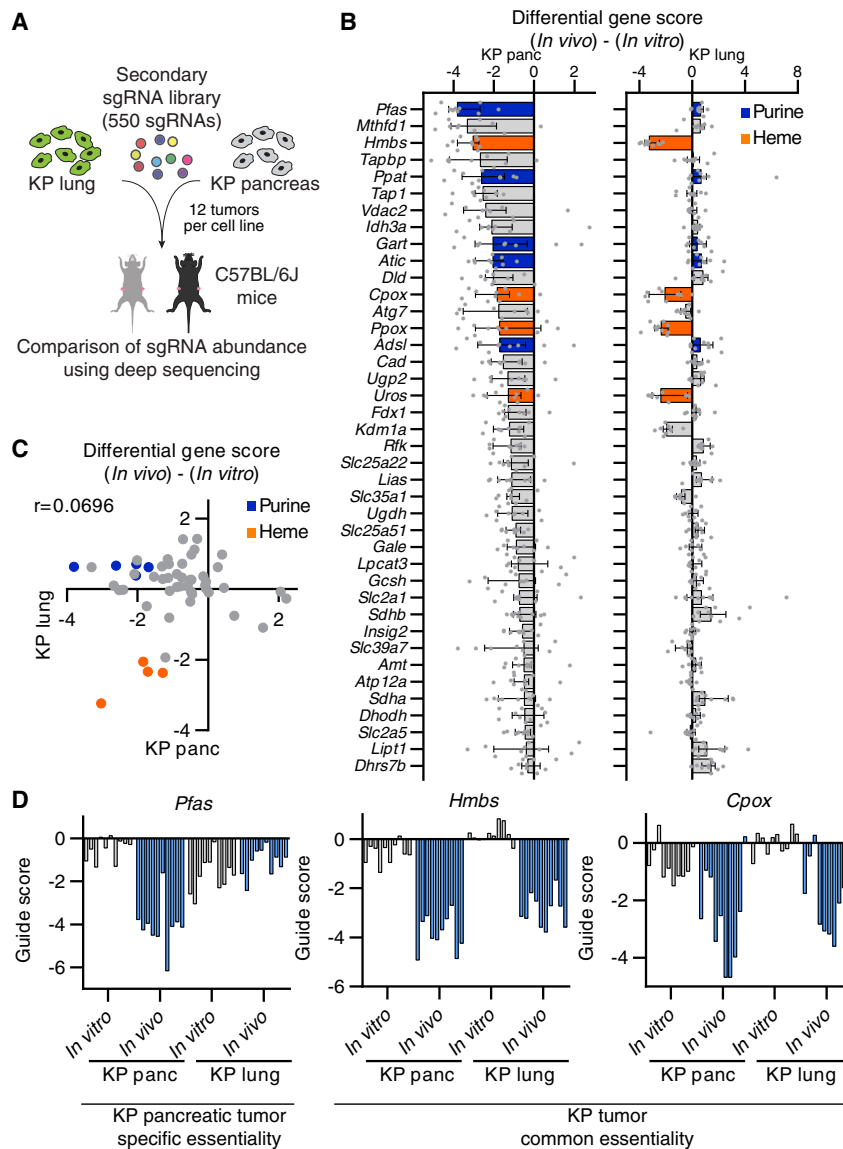


**Figure 2. Metabolic Essentialities in *Kras*-Driven Cancers Are Partly Dictated by Tissue of Origin**

(A) Schematic of focused genetic screens to identify common and different essential metabolic genes for KP pancreatic and KP lung tumor growth *in vivo*. (B) Top 40 genes scoring as differentially required *in vivo* in pancreatic tumors aligned to their differential gene scores in KP lung tumors. Genes involved in purine or heme synthesis are indicated. Bars are median differential gene scores with interquartile range. Dots are individual differential guide scores. (C) Gene scores of *in vivo* KP pancreas tumor growth versus KP lung tumor growth in C57BL/6J mice. Genes involved in purine or heme synthesis are indicated. (D) Guide scores of the indicated genes in the focused *in vivo* screens from KP pancreas and KP lung tumors.

essential, in line with findings that oncogenic *Kras* supports pancreatic cancer through regulation of nucleotide synthesis and inhibition of nucleotide metabolism slows down tumor growth *in vivo* (Santana-Codina et al., 2018). Finally, PDACs display high basal autophagic flux (Yang et al., 2011, 2014, 2018), inhibition of which decreases tumorigenicity *in vivo*. Interestingly, consistent with the higher lipid content of the serum *in vivo* (Weiss et al., 1986), several lipid synthesis genes, such as ATP citrate lyase (*Acly*) and hydroxysteroid 17-beta dehydrogenase 12 (*Hsd17b12*), known to be essential for cancer cell growth in culture were dispensable for tumor growth (Figures S1B and S1C). Reflecting these recently reported vulnerabilities, our screens provide a robust compendium of metabolic

and culture systems, a substantial fraction of metabolic essentialities of pancreatic cancer cells are similar and likely not determined by the tumor environment.

Our screens also identify a small fraction of metabolic genes that are differentially required during tumor formation (~200 genes, ~7% of all screened genes) (Figure 1D). iPAGE analysis (Goodarzi et al., 2009) to search for the pathways most informative about the observed gene essentiality differences reveals that *in vivo* metabolic dependencies were enriched with gene modules associated with heme metabolism, oxidative phosphorylation, nucleotide synthesis, and antigen presentation (Figures 1D and 1E). Among these are several metabolic genes previously reported to be selectively essential in tumors. For example, glucose transporters (*Slc2a1*) and electron transport chain components are necessary to enable cancer cell proliferation only under low-glucose conditions of the tumor environment (Birsoy et al., 2014). Notably, genes involved in purine and pyrimidine metabolism such as *Dhodh* and *Ppat* score as

dependencies of pancreatic cancer cells in culture and as tumors.

### The Tissue of Origin Partly Dictates Metabolic Essentialities in *Kras*-Driven Cancers

While environment may impact metabolic phenotypes of tumors, metabolic differences may also result from cell-autonomous factors such as driver mutations or tissue of origin. To address this for tissue of origin, we asked what portion of the metabolic dependencies of *Kras*-driven pancreatic cancer cells are shared by murine lung cancer cell lines with similar mutational profile. We therefore customized a highly focused sgRNA library encompassing only the top scoring guides in our initial screen (top 40 *in vivo* essential genes, top 10 *in vitro* essential genes with 10 sgRNAs per gene and 20 non-targeting control guides) (Figure 2A) and performed a similar screen in a *Kras*-driven lung cancer cell line. The use of a small focused library enables the use of multiple tumor types and better representation of sgRNAs.

Surprisingly, comparison of sgRNA abundance reveals that only few of the metabolic essentialities were similar between the *Kras*-driven pancreas and lung cancer cells, suggesting that tissue of origin is an important determinant for metabolic dependencies *in vivo* (Figures 2B and 2C). Specifically, most metabolic dependencies of *Kras*-driven pancreatic tumors such as purine synthesis and autophagy were not differentially essential in *Kras*-driven lung tumors (Figure 2D). These findings are also consistent with previous work where tissue context dictates the use of different metabolic routes in mutant *Kras*-driven cancers (Mayers et al., 2016). Interestingly, among these, sgRNAs for heme synthesis genes (*Uros*, *Cpox*, *Ppox*, and *Hmbs*) were depleted in both lung and pancreas tumors, indicating a generalized environmental pressure imposing the heme dependency regardless of tissue of origin (Figures 2B–2D). Given the uncharacterized role of heme metabolism in pancreas cancer and its high score, we next focused our attention on heme synthesis.

### Heme Synthesis Is a Metabolic Dependency of *Kras*-Driven Cancer Cells Specifically *In Vivo*

Our screens yielded heme synthesis as the only common metabolic essentiality *in vivo* for lung and pancreatic cancer growth, raising the possibility that a common environmental limitation may impose this dependency. Consistent with the screening results, while depletion of *Hmbs* showed only a modest effect on the proliferation of these cancer cell lines in culture (Figures 3A and 3B), *Hmbs* loss strongly reduced the sizes of the tumors *in vivo* (Figure 3C). As heme acts as a cofactor for several enzymes of the electron transport chain (ETC) (Fukuda et al., 2017; Lin et al., 2019), the slight defect in cell growth *in vitro* could be exacerbated when cells were seeded at a low confluency and could be rescued by the addition of hemin (oxidized heme), pyruvate, or the expression of LbNOX, an NADH oxidase that increases NAD<sup>+</sup>/NADH ratio (Titov et al., 2016) (Figures S2A–S2D).

We next asked why cancer cells require heme synthesis specifically in the tumor environment and which environmental factors *in vivo* may result in this dependency. Heme limitation in tumors may be a result of lower heme availability or an increase in heme degradation (Li and Stocker, 2009). In line with the latter possibility, we observed substantial upregulation of heme oxygenase 1 (Hmox1), the rate-limiting enzyme in heme catabolism, in tumors and in hypoxia compared to cultured cancer cells in normoxia (Figure 3D). Heme catabolism and Hmox1 upregulation are highly associated with oxidative stress and hypoxia, conditions observed in the tumor microenvironment (Panchenko et al., 2000). While hypoxia-inducible factor (HIF) regulates many of the cancer cell responses under hypoxia, knocking out *Hif1a* or *Hif2a* did not prevent Hmox1 stabilization in this context (Figure S2E). Building upon these observations, we hypothesized that upregulation of Hmox1 proteins, though normally beneficial for tumors (Figures S2F–S2H), likely makes heme a limiting molecule for tumor growth due to increased heme degradation. To test this possibility, we knocked out *Hmox1* in murine pancreatic cancer cells deficient for *Hmbs* and asked whether heme becomes a limiting metabolite for growth. Supporting this idea, blocking heme degradation by knocking out *Hmox1* partially rescued growth inhibition of tumors expressing *Hmbs* sgRNAs (Figures 3E and 3F).

To translate our findings to a more relevant *in vivo* model, we next asked whether targeting heme synthesis impacts the growth of patient-derived xenografts (PDXs). For this, we performed an *in vivo* loss-of-function competition assay using a pool of sgRNAs targeting control genomic regions or the *HMBS*, *CPOX* heme synthesis genes, and *PPAT* purine synthesis gene as a positive control. Consistently, sgRNAs targeting the heme synthesis genes, but not those of controls, strongly inhibited the growth of tumors derived from the *KRAS* mutant pancreas PDXs (Figure 3G). Notably, using heme synthesis genes as a combined signature for scoring samples in the TCGA-PAAD dataset revealed a significant association between higher expression of heme synthesis genes and lower disease-free survival compared to the group with lower expression ( $p = 0.05$ ) (Figure 3H). Taken together, our results identify heme synthesis as a metabolic liability imposed by the tumor microenvironment, independent of tissue of origin.

### Identification of Metabolic Genes that Are Essential for Pancreatic Cancer Immune Evasion

We next asked whether any of the *in vivo* essential genes scored due to the presence of the immune system. As pancreatic tumors have immunosuppressive environments and are generally resistant to immunotherapy (Ryan et al., 2014), we hypothesized that a subset of the scoring metabolic genes may be involved in immune evasion and that their loss should enhance immune-mediated killing of cancer cells. To identify such genes, we repeated our genetic screens in immunodeficient NOD-SCID gamma (NSG) mice lacking mature T, B, and natural killer (NK) cells and compared these hits to those obtained in immunocompetent mice (Figure 4A). Confirming the robustness of the screens, most genes scored similarly with a correlation of  $r = 0.892$  (Figure 4B).

Among the top genes differentially essential for tumor growth in immunocompetent mice were *Tap1* and *Tapbp*, genes required for the loading of antigen-derived peptides onto major histocompatibility complex (MHC) class I molecules for presentation (Figures 4B and 4C). In previously published work, loss of Tap proteins strongly blocks CD8<sup>+</sup> T cell-mediated killing of cancer cells in co-culture assays *in vitro* (Kearney et al., 2018; Patel et al., 2017). However, our *in vivo* screens suggest that loss of key MHC class I-related genes has an opposite effect possibly because loss of MHC class I expression downstream of *Tap1* (Figure S3A) and *Tapbp* deletion can promote the killing of tumor cells by NK cells (Wu and Lanier, 2003). The only other hit from our screen was *Atg7*, a key enzyme involved in macroautophagy (Figures 4B and 4C). Of note, a similar autophagy gene, *Atg5*, also scored in our initial screen (Figure S3B; Table S1), raising the possibility that autophagy may be a key process for immune evasion or immune-mediated cell death. As our screens did not result in any high-scoring metabolic pathways in anabolic or catabolic pathways other than autophagy, these results argue that cancer cell metabolism may not be a major driver for immune evasion in mouse pancreatic cancers.

Pancreatic cancer cells display elevated autophagy, inhibition of which suppresses tumor growth in xenografts (Guo et al., 2011; Perera et al., 2015) and genetically engineered mouse models (GEMMs) (Yang et al., 2011, 2014, 2018). While several mechanisms have been proposed regarding how autophagy

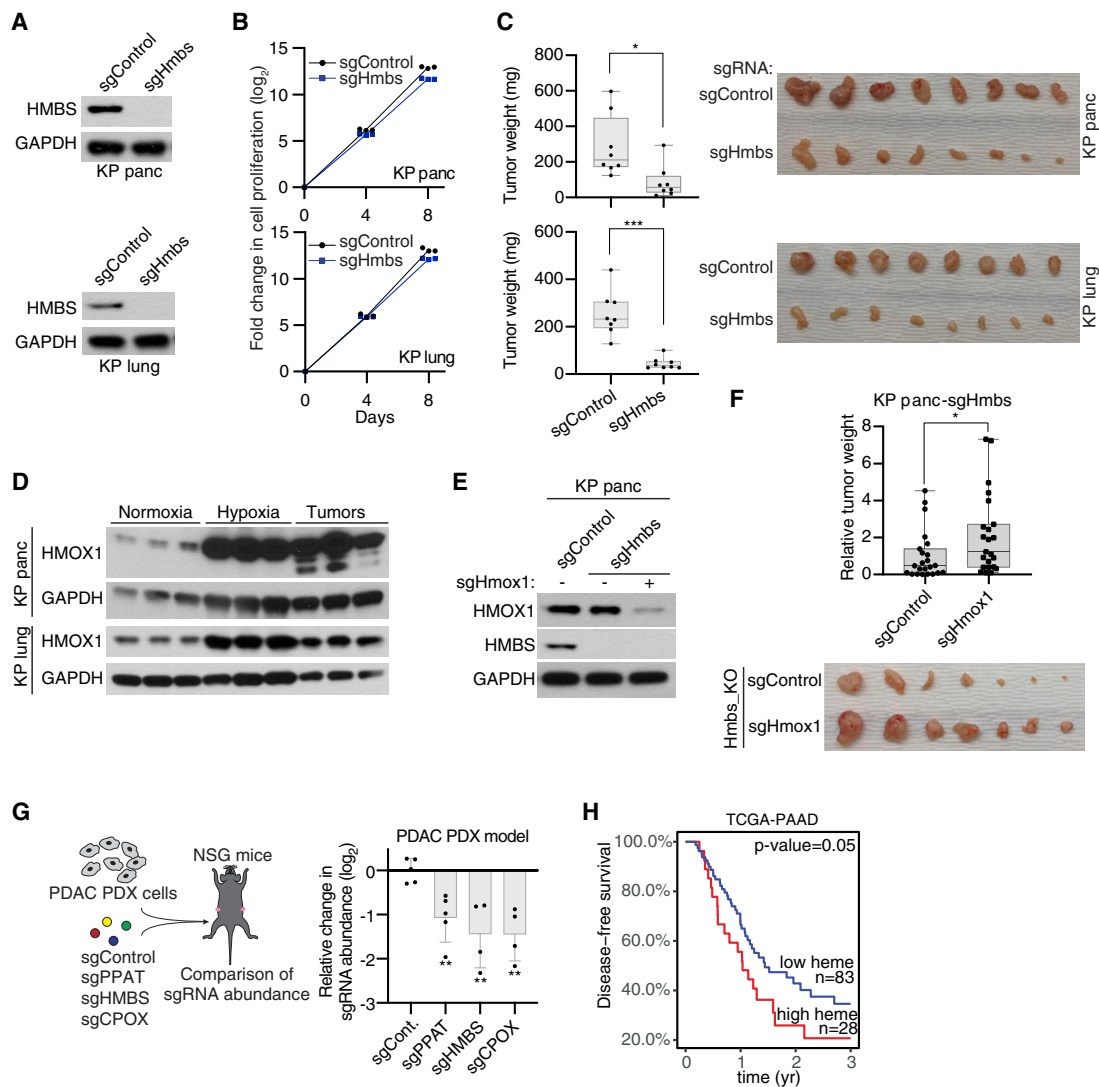


**Figure 3. Heme Synthesis Is a Metabolic Dependency of *Kras*-Driven Tumors *In Vivo***

(A) Immunoblot of HMBS in the indicated KP pancreas and KP lung cancer cell lines. GAPDH was used as loading control.  
 (B) Fold change in cell number ( $\log_2$ ) of the indicated KP pancreas and KP lung cancer cell lines after culturing *in vitro* for the indicated durations (mean  $\pm$  SD,  $n = 3$ ). \*\*\* $p < 0.001$  versus sgControl.  
 (C) Tumor weights of the indicated KP pancreas and KP lung tumors engrafted subcutaneously in C57BL/6J mice (box and whisker,  $n = 8$ ). \* $p < 0.05$ , \*\*\* $p < 0.001$  versus sgControl (left). Images of the indicated KP pancreas and KP lung tumors (right).  
 (D) Immunoblot of HMOX1 in KP pancreas and KP lung cancer cells grown *in vitro* under normoxia, under hypoxia (0.5% oxygen) for 48 h, and in subcutaneous tumors. GAPDH was used as loading control.  
 (E) Immunoblots of HMOX1 and HMBS in the indicated KP pancreas cell lines. GAPDH was used as loading control.  
 (F) Relative tumor weights of the indicated KP pancreas Hmbs\_KO tumors engrafted subcutaneously in C57BL/6J mice (box and whisker,  $n = 23$ ). \* $p < 0.05$  versus control (top). Representative image of the indicated KP pancreas Hmbs\_KO tumors (bottom).  
 (G) Schematic of competition assay using PDAC patient-derived xenograft cells infected with the indicated sgRNAs. Cells were then engrafted subcutaneously in NSG mice (left). Relative fold change in sgRNA abundance ( $\log_2$ ) from the PDX (mean  $\pm$  SD,  $n = 5$ ). \*\* $p < 0.01$  versus sgControl (right).  
 (H) Disease-free survival rates of TCGA PDAC patients with high or low heme synthesis gene expressions. Weighted average expressions of CPOX, HMBS, PPOX, and UROS were used (low heme  $n = 83$ , high heme  $n = 28$ ).

See also [Figure S2](#).

sustains pancreatic tumor growth (Amaravadi et al., 2016), the precise reason for the autophagy dependency of PDACs is not fully understood. Consistent with the previous findings, macroautophagy was dispensable for the growth of *Kras* mutant pancreatic cancer cells in culture (Eng et al., 2016) (Figure S3B). In contrast, *Atg7*-deficient tumors in immunocompetent C57BL/

6J mice were substantially smaller compared to those expressing sgRNA-resistant *Atg7* cDNA (Figures 4D and 4E). Remarkably, this difference is dependent on the presence of lymphocytes, as the effect is completely abolished in NSG mice and mostly lost in Rag1 null mice, which lack mature T and B cells, but not NK cells (Figures 4E and S3C). Similar to

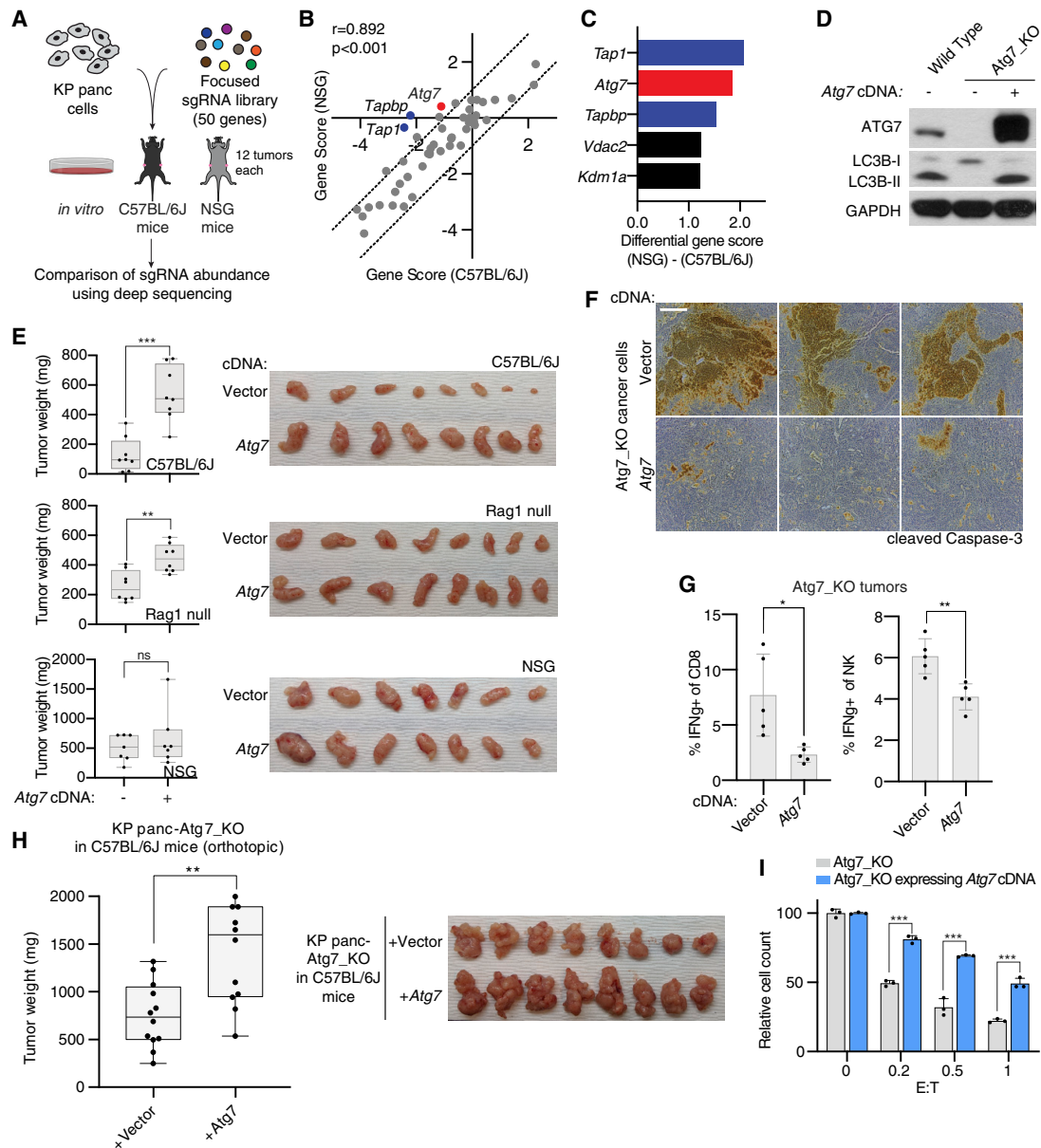


**Figure 4. Autophagy is an Immune-Dependent Metabolic Liability and Enables Immune Evasion in PDAC**

(A) Schematic of focused genetic screens to identify immune-dependent metabolic liabilities of KP pancreatic tumor growth *in vivo*.

(B) Gene scores of *in vivo* KP pancreas tumor growth in immunodeficient NSG mice versus immunocompetent C57BL/6J mice.

(C) Top 5 genes scoring as differentially required for KP pancreas tumor growth in immunocompetent mice compared to immunodeficient mice. Genes involved in TAP complex are indicated in blue. The autophagy gene *Atg7* is indicated in red.

(D) Immunoblots of ATG7 and LC3B in the indicated KP pancreas cell lines. GAPDH was used as loading control.

(E) Tumor weights of the indicated KP pancreas *Atg7*\_KO tumors engrafted subcutaneously in the indicated mice (box and whisker,  $n=8$ ).  $**p<0.01$ ,  $***p<0.001$  versus *Atg7* addback (left). Image of the indicated KP pancreas *Atg7*\_KO tumors from the indicated mice (right).

(F) Immunohistochemical staining of cleaved-CASPASE-3 in the indicated KP pancreas *Atg7*\_KO tumors engrafted subcutaneously in C57BL/6J mice. Representative images are shown. Scale bar, 230  $\mu\text{m}$ .

(G) Percentage of IFN $\gamma$ + activated CD8+ T cells (left) and NK cells (right) extracted from the indicated KP pancreas *Atg7*\_KO tumors engrafted subcutaneously in C57BL/6J mice (mean  $\pm$  SD,  $n=5$ ).  $*p<0.05$ ,  $***p<0.001$  versus *Atg7* addback.

(H) Tumor weights of the indicated KP pancreas *Atg7*\_KO tumors engrafted orthotopically in the pancreas of C57BL/6J mice (box and whisker,  $n=12$ ).  $**p<0.01$  versus *Atg7* addback (left). Representative image of the orthotopic KP pancreas *Atg7*\_KO tumors from the indicated mice (right).

(I) Relative cell count of the indicated OVA-expressing KP pancreas *Atg7*\_KO cell lines after co-culturing with activated OT-I CD8+ T cells for 48 h at the indicated E:T ratios (mean  $\pm$  SD,  $n=3$ ). Counts were normalized to the average of the monocultured cells of the same line.  $***p<0.001$  versus *Atg7* addback.

See also [Figure S3](#).

the mouse pancreatic cell line, *ATG7* loss in human *KRAS* mutant pancreatic tumors did not reduce tumor growth in NSG mice (Figures S3D and S3E). Immunohistochemical staining of tumor sections and immunoblotting showed increased caspase-3 cleavage in *Atg7*-deficient tumors (Figures 4F and S3F), suggesting an immune-mediated increase in cell death. While we did not observe any increase in CD8+ T cell infiltration into *Atg7*-deficient tumors (Figure S3G) or increases in the proportions of CD8+, CD4+, or NK cells within the infiltrating immune cells (Figures S3H–S3J), immune profiling showed an increase in IFN $\gamma$  expression by both CD8+ T cells and NK cells (Figures 4G and S3K), in line with the small but significant decrease of tumor size in Rag1 null mice and the larger decrease in NSG mice. Notably, *ATG7* expression may be a predictive factor for patient outcomes, as pancreas cancer patients with low *ATG7* expression have significantly higher disease-free survival rates compared to patients with high *ATG7* expression (Figure S3L). A similar growth difference between *Atg7*-deficient and proficient cells was observed in orthotopically injected tumors in the pancreas of C57BL/6J mice (Figure 4H). Finally, consistent with the increased IFN $\gamma$  expression by CD8+ T cells, loss of *Atg7* sensitized pancreatic cancer cells expressing ovalbumin (OVA) antigen to OT-I T cell receptor-transgenic CD8+ T cell-mediated killing in co-culture experiments (Figures 4I, S3M, and S3N). Altogether, these results support a role for autophagy in PDAC immune evasion.

### Autophagy Enables Tumor Immune Evasion and Protects against TNF $\alpha$ -Induced Apoptosis

We next sought to understand how *Atg7* loss would enhance immune cell-mediated killing in pancreatic cancer cells. As presentation of neoantigens by MHC class I molecules enables detection of cancer cells by CD8+ T cells, autophagy inhibition may disrupt antigen presentation and promote immune evasion, as previously suggested (Loi et al., 2016; Yamamoto et al., 2020). However, we did not detect substantial differences in MHC-I protein levels or surface expression in either mouse or a subset of human pancreatic cancer cell lines when stimulated with IFN $\gamma$  (Figures S4A–S4H). Autophagy inhibition has also been suggested to increase the expression of programmed death-ligand 1 (PD-L1) (Wang et al., 2019), but we did not observe any change in surface PD-L1 upon loss of autophagy (Figure S4I). To investigate alternative pathways that may lead to resistance to immune-mediated killing, we analyzed the transcriptome of *Atg7*-deficient tumors and their isogenic counterparts complemented with *Atg7* cDNA using RNA sequencing. Remarkably, iPAGE analysis revealed a strong enrichment for immune response pathways that are upregulated upon autophagy loss including gene sets that respond to TNF $\alpha$  or IFN $\gamma$ , raising the possibility that *Atg7* loss may enhance the sensitivity of tumor cells to these cytokines (Figures 5A and S4J–S4L; Table S2).

Building upon this observation, we asked whether autophagy protects cancer cells from cytokine-mediated cytotoxicity. Cell growth assays of pancreatic cancer cell lines with cytokines revealed that autophagy null PDAC cells are oversensitive to TNF $\alpha$ , but not to IFN $\gamma$  (Figures 5B, 5C, and S5A), and undergo Rip1-independent apoptosis upon TNF $\alpha$  treatment as assessed by immunoblotting of caspase-8 and caspase-3 cleavage (Figures 5D and S5B–S5D). While a change in the surface

expression of the canonical receptor Tnfrsf1a may explain the protective effect of autophagy, we did not observe any differences in protein or surface expression levels of Tnfrsf1a in *Atg7* null cells (Figures 5E and S5E). Furthermore, CRISPR-mediated knockout of the canonical receptor *Tnfrsf1a* completely abolished the sensitivity of autophagy-deficient cells to TNF $\alpha$  (Figure 5E). Knockout of the alternate receptor *Tnfrsf1b* did not affect the sensitivity of autophagy-deficient cells (Figure S5F), suggesting that autophagy may be specifically regulating the downstream response to Tnfrsf1a. This effect could also be recapitulated through pharmacological inhibition of autophagy with bafilomycin A1 or in autophagy-deficient KP lung cancer cells and was independent of any secreted factors, supporting a generalized cell-autonomous link between autophagy and TNF $\alpha$  sensitivity (Figures 5G and S5G–S5I). Notably, consistent with both pro-apoptotic and pro-survival effects of TNF $\alpha$  signaling on tumors *in vivo* (Wang and Lin, 2008), expression of *Tnfrsf1a* sgRNAs in the pancreatic cancer cells severely reduced tumor growth regardless of autophagy proficiency (Figure S5J).

Finally, we tested whether TNF $\alpha$  sensitivity accounts for the increased T cell killing of autophagy-deficient mouse pancreatic cancer cells in an antigen-specific *in vitro* co-culture assay. Specifically, we used an OVA antigen-expressing pancreatic cancer cell line as a target cell and OT-I CD8+ T cells as the effector cells. *Atg7* null cells and their *Atg7*-expressing counterparts were co-cultured with OT-I CD8+ T cells for 48 h in the presence or absence of a neutralizing anti-mouse TNF $\alpha$  antibody. The remaining live cancer cells were counted after co-culture and revealed that the oversensitivity of autophagy-deficient cancer cells to CD8+ T cells was completely rescued by addition of the anti-TNF $\alpha$  neutralizing antibody (Figure 5H). Altogether, these results suggest that autophagy protects PDAC cells from cell death resulting from TNF $\alpha$  secreted by immune cells such as CD8+ T cells.

### Conclusion

Using parallel loss-of-function screens, our study provides a comparative compendium of metabolic dependencies of pancreatic cancer cells grown in culture and as tumors. Surprisingly, the high degree of correlation between metabolic essentialities *in vitro* and *in vivo* suggests that culture conditions may recapitulate a substantial portion of the metabolic dependencies in tumors and may provide a reasonable approximation to study cancer metabolism. However, our work also identifies a subset of metabolic dependencies unique to the tumor environment and shared by both *Kras* mutant pancreatic and lung cancer cells. In particular, we discovered heme synthesis as a common metabolic liability in tumors, indicating the significance of recent efforts to better model tumor nutrient conditions (Cantor et al., 2017; Vande Voorde et al., 2019). This is likely due to upregulation of Hmox1 through hypoxia or ROS, which imposes a stronger demand for heme availability in subcutaneously engrafted tumors. Interestingly, Hmox1 has previously been shown to be regulated by multiple stress conditions and signaling pathways (Alam and Cook, 2007). For example, lung tumors upregulate Hmox1 through activation of NRF2, the master regulator of the antioxidant response pathway (Lignitto et al., 2019). Despite

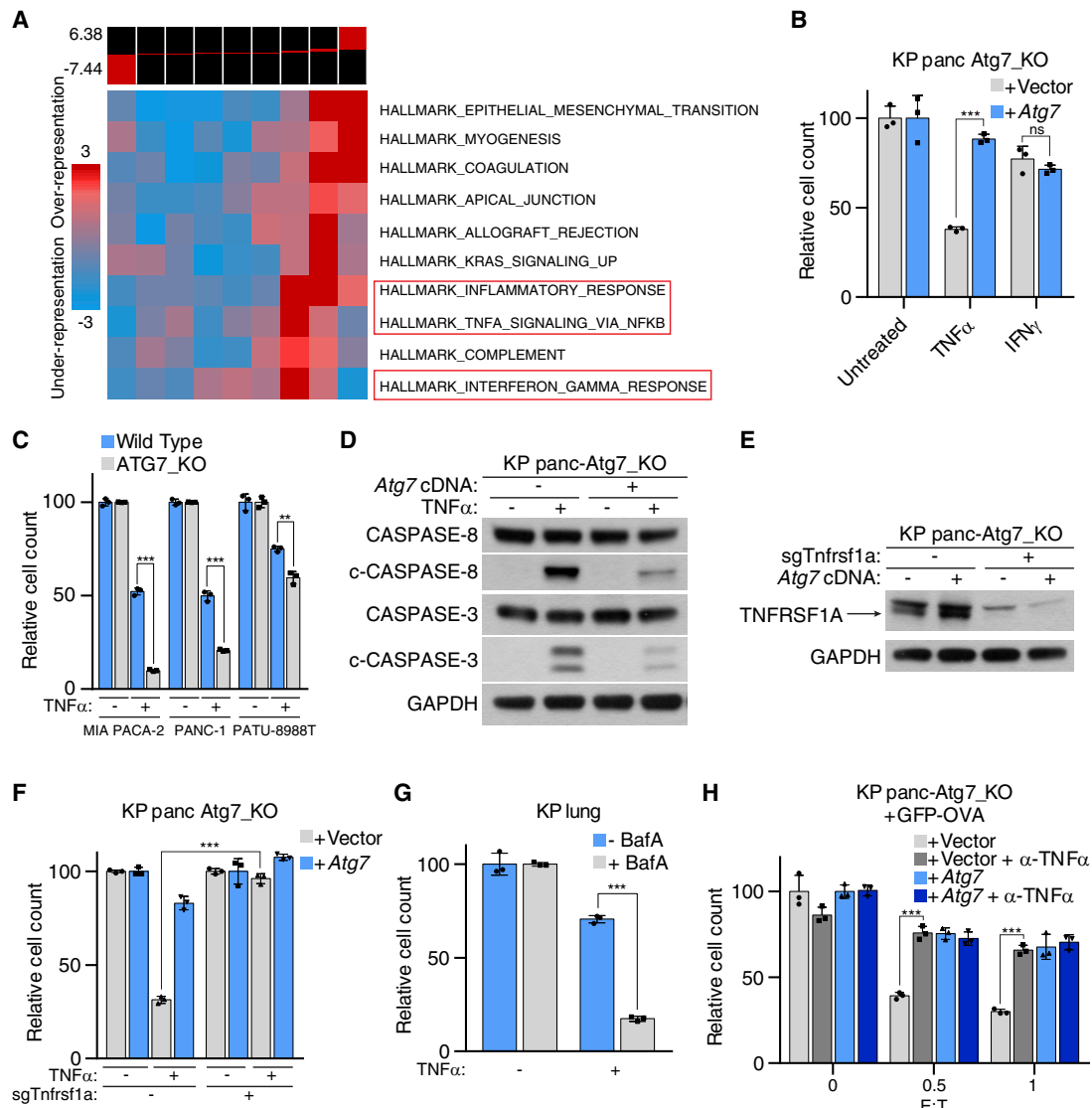


**Figure 5. Autophagy Enables Tumor Immune Evasion by Increasing TNF $\alpha$  Resistance**

(A) RNA sequencing analysis of KP pancreas Atg7\_KO tumors. Gene sets enriched in transcriptome of KP pancreas Atg7\_KO tumors compared to Atg7 addback tumors engrafted subcutaneously in C57BL/6J mice (n = 3). Immune-related gene sets are boxed in red.

(B) Relative cell count of indicated KP pancreas Atg7\_KO cell lines treated for 48 h with 100 ng/mL TNF $\alpha$  or 100 ng/mL IFN $\gamma$  (mean  $\pm$  SD, n = 3). Counts were normalized to the average of the untreated cells of the same line. \*\*\*p < 0.001 versus Atg7 addback.

(C) Relative cell count of indicated human pancreatic cancer MIA PaCa-2, PANC-1, and PATU-8988T cell lines treated for 48 h with 100, 200, and 600 ng/mL TNF $\alpha$ , respectively (mean  $\pm$  SD, n = 3). Counts were normalized to the average of the untreated cells of the same line. \*\*p < 0.01, \*\*\*p < 0.001 versus wild type.

(D) Immunoblot of CASPASE-8, cleaved CASPASE-8, and CASPASE-3 in the indicated KP pancreas Atg7\_KO cell lines treated for 24 h with 100 ng/mL TNF $\alpha$ . GAPDH was used as loading control.

(E) Immunoblot of TNFRSF1A in the indicated KP pancreas Atg7\_KO cell lines. GAPDH was used as loading control.

(F) Relative cell count of indicated KP pancreas Atg7\_KO cell lines treated for 48 h with 100 ng/mL TNF $\alpha$  (mean  $\pm$  SD, n = 3). Counts were normalized to the average of the untreated cells of the same line. \*\*\*p < 0.001.

(G) Relative cell count of KP pancreas cells treated for 48 h with 100 ng/mL TNF $\alpha$  or 50 nM Bafilomycin A1 (BafA) (mean  $\pm$  SD, n = 3). Counts were normalized to the average of the untreated cells or those treated with BafA only. \*\*\*p < 0.001.

(H) Relative cell count of the indicated OVA-expressing KP pancreas Atg7\_KO cell lines after co-culturing with activated OT-I CD8+ T cells for 48 h at the indicated E:T ratios with or without 40  $\mu$ g/mL anti-TNF $\alpha$  (mean  $\pm$  SD, n = 3). Counts were normalized to the average of the untreated monocultured cells of the same line. \*\*\*p < 0.001 versus untreated cells.

See also [Figures S4](#) and [S5](#).

this, the precise mechanism for Hmox1 upregulation in different tumor contexts remains to be identified.

Consistent with the strong impact of the tissue of origin on metabolism, most dependencies we identified in this work were specific to pancreatic cancer cells and not observed in lung cancers (Vander Heiden and DeBerardinis, 2017). Remarkably, among all the scoring pathways, autophagy was the only metabolic process that enabled pancreatic cancer cells to evade the immune system. While our experiments suggest a protective role for autophagy from TNF $\alpha$ -mediated cell death, previous work suggests that autophagy is also involved in MHC-I presentation and impacts the trafficking of surface MHC-I molecules in a different group of PDAC cell lines (Loi et al., 2016; Yamamoto et al., 2020). Given that the effect of autophagy loss on MHC-I expression is variable in different cell lines, autophagy may enable immune evasion through multiple mechanisms depending on the context. Furthermore, the complexity of the tumor microenvironment does not preclude that a combination of MHC-I presentation and cytokine insensitivity may play a role in immune evasion.

While loss of autophagy increases the TNF $\alpha$  sensitivity of pancreatic cancer cell lines, the exact mechanism of this enhanced sensitivity and how autophagy protects cells from cytokine-mediated death are not well understood. Though several studies have associated autophagy with TNF $\alpha$  signaling in other cell types due to increased necroptosis (Lim et al., 2019) or Rip1-dependent apoptosis (Orvedahl et al., 2019), our results show a similar phenotype in pancreatic cancer cells independent of Rip1. These findings suggest that autophagy may be associated with other downstream TNF $\alpha$  adaptor proteins. TNF $\alpha$  is a multifunctional cytokine that has been shown to both promote and suppress tumor growth in different contexts (Wang and Lin, 2008). Consistent with this, blocking TNF $\alpha$  *in vivo* is disruptive to tumor growth and may mask the effect of autophagy loss on TNF $\alpha$ -mediated apoptosis. Future work is required to determine downstream adaptor proteins, which may improve our understanding of how autophagy protects cells from TNF $\alpha$ -mediated cell death and lead to therapeutic strategies. Since many pancreatic cancers display high autophagic flux and have immunosuppressive environments, we reveal an underappreciated facet of targeting autophagy-associated immunomodulation of pancreatic tumor growth, which may be effectively combined with current immunotherapies. Altogether, our screens reveal metabolic dependencies arising from microenvironmental limitations and the immune system, providing a resource for potential metabolism-based anti-cancer strategies.

### Limitations of Study

We are aware of several limitations to our screening approach. As an *in vivo* screening approach for a comprehensive CRISPR library requires a large number of tumors to achieve efficient representation of guides, we used subcutaneous tumors rather than orthotopic counterparts or GEMMs, which are physiologically more relevant. While it is possible that we may have missed some organ-specific metabolic liabilities, our screens still provide a valuable resource for the comparison of metabolic dependencies of pancreatic cancer cells in culture and *in vivo*. Indeed, the role of autophagy on immune evasion could be recapitulated by orthotopic injections into pancreas. Additionally, it should be

noted that, within large-scale pooled CRISPR screens, we culture a population of knockout cells with those that still express the functional gene product. This heterogeneity may enable the transfer of metabolites and growth factors and may mask certain dependencies under culture conditions. Though we did not observe proliferation defects in autophagy-deficient cells *in vitro*, we do not rule out the possibility that other signaling pathways may be compensating for the metabolic defect (Towers et al., 2019). Finally, the number of cell lines used in this study is limited. Therefore, metabolic limitations and downstream mechanisms we identified may not be generalizable to all KP pancreas and lung tumors. We also mainly used engrafted tumor cells and not GEMMs, which can best recapitulate tumor biology even from an early initiation step. As new screening techniques emerge, more advanced genetic screens, especially in GEMMs, would enable us to better identify metabolic dependencies of individual tumor types in their natural context.

### STAR★METHODS

Detailed methods are provided in the online version of this paper and include the following:

- KEY RESOURCES TABLE
- RESOURCE AVAILABILITY
  - Lead Contact
  - Materials Availability
  - Data and Code Availability
- EXPERIMENTAL MODEL AND SUBJECT DETAILS
  - Cell Culture
  - Mouse Studies
- METHOD DETAILS
  - CRISPR-based Screens
  - Immunoblot
  - Generation of Knock-out and cDNA Overexpression Cell Lines
  - Cell Proliferation and Survival Assays
  - Patient-Derived Pancreatic Cancer Xenografts
  - Immunohistochemistry
  - Immune Profiling of Tumors
  - OT-I T Cell Co-culture
  - Flow Cytometry
  - RNaseq
  - Survival Analysis
  - Immunofluorescence
- QUANTIFICATION AND STATISTICAL ANALYSIS

### SUPPLEMENTAL INFORMATION

Supplemental Information can be found online at <https://doi.org/10.1016/j.cmet.2020.10.017>.

### ACKNOWLEDGMENTS

We thank all members of the Birsoy Lab for helpful suggestions. We would like to thank members of the Rockefeller University Genomics Resource Center, Proteomics Resource Center, Bio-Imaging Resource Center, Flow Cytometry Resource Center, and Weill Cornell Laboratory of Comparative Pathology for their assistance. We also thank Sohail Tavazoie for his scientific input. This research is supported by the NIH Director's New Innovator Award (DP2 CA228042-01) (K.B.), Pershing Square Sohn Foundation (K.B.), the 2017

Breast Cancer Research Foundation-AACR NextGen Grant for Transformative Cancer Research in honor of Dr. Nancy E. Davidson, grant number 17-20-26-BIRS (K.B.), and Robertson Therapeutic Development Fund (X.G.Z.). X.G.Z. is supported by the Sackler Center for Biomedicine and Nutrition Research through the generosity of the Sackler Foundation. K.B. is a Searle Scholar, Pew-Stewart Scholar, and Sidney Kimmel Scholar.

#### AUTHOR CONTRIBUTIONS

Conceptualization, K.B. and X.G.Z.; Methodology, K.B., X.G.Z., G.D.V., and H.G.; Formal Analysis, A.A., S.H., and H.M.; Investigation, X.G.Z., A.C., L.B., B.P., Y.L., B.N.O., N.Y., B.T., and R.T.; Resources, E.d.S.; Writing – Original Draft, X.G.Z. and K.B.; Writing – Review & Editing, X.G.Z. and K.B.; Funding Acquisition, K.B. and X.G.Z.

#### DECLARATION OF INTERESTS

K.B. is scientific advisor to Nanocare Pharmaceuticals and a consultant to Barer Institute.

Received: April 28, 2020

Revised: August 12, 2020

Accepted: October 19, 2020

Published: November 4, 2020

#### REFERENCES

Alam, J., and Cook, J.L. (2007). How many transcription factors does it take to turn on the heme oxygenase-1 gene? *Am. J. Respir. Cell Mol. Biol.* **36**, 166–174.

Alvarez, S.W., Sviderskiy, V.O., Terzi, E.M., Papagiannakopoulos, T., Moreira, A.L., Adams, S., Sabatini, D.M., Birsoy, K., and Possemato, R. (2017). NFS1 undergoes positive selection in lung tumours and protects cells from ferroptosis. *Nature* **551**, 639–643.

Amaravadi, R., Kimmelman, A.C., and White, E. (2016). Recent insights into the function of autophagy in cancer. *Genes Dev.* **30**, 1913–1930.

Badgley, M.A., Kremer, D.M., Maurer, H.C., DelGiorno, K.E., Lee, H.-J., Purohit, V., Sagalovskiy, I.R., Ma, A., Kapilian, J., Firl, C.E.M., et al. (2020). Cysteine depletion induces pancreatic tumor ferroptosis in mice. *Science* **368**, 85–89.

Birsoy, K., Possemato, R., Lorbeer, F.K., Bayraktar, E.C., Thiru, P., Yucel, B., Wang, T., Chen, W.W., Clish, C.B., and Sabatini, D.M. (2014). Metabolic determinants of cancer cell sensitivity to glucose limitation and biguanides. *Nature* **508**, 108–112.

Birsoy, K., Wang, T., Chen, W.W., Freinkman, E., Abu-Remaileh, M., and Sabatini, D.M. (2015). An essential role of the mitochondrial electron transport chain in cell proliferation is to enable aspartate synthesis. *Cell* **162**, 540–551.

Cantor, J.R., Abu-Remaileh, M., Kanarek, N., Freinkman, E., Gao, X., Louissaint, A., Jr., Lewis, C.A., and Sabatini, D.M. (2017). Physiologic medium rewires cellular metabolism and reveals uric acid as an endogenous inhibitor of UMP synthase. *Cell* **169**, 258–272.e17.

Eng, C.H., Wang, Z., Tkach, D., Toral-Barza, L., Ugwonali, S., Liu, S., Fitzgerald, S.L., George, E., Frias, E., Cochran, N., et al. (2016). Macroautophagy is dispensable for growth of KRAS mutant tumors and chloroquine efficacy. *Proc. Natl. Acad. Sci. USA* **113**, 182–187.

Faubert, B., Li, K.Y., Cai, L., Hensley, C.T., Kim, J., Zacharias, L.G., Yang, C., Do, Q.N., Doucette, S., Burguete, D., et al. (2017). Lactate metabolism in human lung tumors. *Cell* **171**, 358–371.e9.

Fukuda, Y., Wang, Y., Lian, S., Lynch, J., Nagai, S., Fanshawe, B., Kandilci, A., Janke, L.J., Neale, G., Fan, Y., et al. (2017). Upregulated heme biosynthesis, an exploitable vulnerability in MYCN-driven leukemogenesis. *JCI Insight* **2**, e92409.

Garcia-Bermudez, J., Baudrier, L., Bayraktar, E.C., Shen, Y., La, K., Guarecuco, R., Yucel, B., Fiore, D., Tavora, B., Freinkman, E., et al. (2019). Squalene accumulation in cholesterol auxotrophic lymphomas prevents oxidative cell death. *Nature* **567**, 118–122.

Goodarzi, H., Elemento, O., and Tavazoie, S. (2009). Revealing global regulatory perturbations across human cancers. *Mol. Cell* **36**, 900–911.

Guo, J.Y., Chen, H.-Y., Mathew, R., Fan, J., Strohecker, A.M., Karsli-Uzunbas, G., Kamphorst, J.J., Chen, G., Lemons, J.M.S., Karantza, V., et al. (2011). Activated Ras requires autophagy to maintain oxidative metabolism and tumorigenesis. *Genes Dev.* **25**, 460–470.

Hui, S., Ghergurovich, J.M., Morscher, R.J., Jang, C., Teng, X., Lu, W., Esparza, L.A., Reya, T., Le Zhan, Yanxiang Guo, J., et al. (2017). Glucose feeds the TCA cycle via circulating lactate. *Nature* **557**, 115–118.

Kearney, C.J., Vervoort, S.J., Hogg, S.J., Ramsbottom, K.M., Freeman, A.J., Lalaoui, N., Pijpers, L., Michie, J., Brown, K.K., Knight, D.A., et al. (2018). Tumor immune evasion arises through loss of TNF sensitivity. *Sci. Immunol.* **3**, eaar3451.

Kishton, R.J., Sukumar, M., and Restifo, N.P. (2017). Metabolic regulation of T cell longevity and function in tumor immunotherapy. *Cell Metab.* **26**, 94–109.

Li, C., and Stocker, R. (2009). Heme oxygenase and iron: from bacteria to humans. *Redox Rep.* **14**, 95–101.

Lignitto, L., LeBoeuf, S.E., Homer, H., Jiang, S., Askenazi, M., Karakousi, T.R., Pass, H.I., Bhutkar, A.J., Tsirigos, A., Ueberheide, B., et al. (2019). Nrf2 activation promotes lung cancer metastasis by inhibiting the degradation of Bach1. *Cell* **178**, 316–329.e18.

Lim, J., Park, H., Heisler, J., Maculins, T., Roose-Girma, M., Xu, M., McKenzie, B., van Lookeren Campagne, M., Newton, K., and Murthy, A. (2019). Autophagy regulates inflammatory programmed cell death via turnover of RHIM-domain proteins. *eLife* **8**, e44452.

Lin, K.H., Xie, A., Rutter, J.C., Ahn, Y.R., Lloyd-Cowden, J.M., Nichols, A.G., Soderquist, R.S., Koves, T.R., Muoio, D.M., MacIver, N.J., et al. (2019). Systematic dissection of the metabolic-apoptotic interface in AML reveals heme biosynthesis to be a regulator of drug sensitivity. *Cell Metab.* **29**, 1217–1231.e7.

Loi, M., Müller, A., Steinbach, K., Niven, J., Barreira da Silva, R., Paul, P., Ligeon, L.-A., Caruso, A., Albrecht, R.A., Becker, A.C., et al. (2016). Macroautophagy proteins control MHC class I levels on dendritic cells and shape anti-viral CD8(+) T cell responses. *Cell Rep.* **15**, 1076–1087.

Mayers, J.R., Torrence, M.E., Danaei, L.V., Papagiannakopoulos, T., Davidson, S.M., Bauer, M.R., Lau, A.N., Ji, B.W., Dixit, P.D., Hosios, A.M., et al. (2016). Tissue of origin dictates branched-chain amino acid metabolism in mutant Kras-driven cancers. *Science* **353**, 1161–1165.

Minton, D.R., Nam, M., McLaughlin, D.J., Shin, J., Bayraktar, E.C., Alvarez, S.W., Sviderskiy, V.O., Papagiannakopoulos, T., Sabatini, D.M., Birsoy, K., and Possemato, R. (2018). Serine catabolism by SHMT2 is required for proper mitochondrial translation initiation and maintenance of formylmethionyl-tRNAs. *Mol. Cell* **69**, 610–621.e5.

Ohtsubo, K., and Marth, J.D. (2006). Glycosylation in cellular mechanisms of health and disease. *Cell* **126**, 855–867.

Orvedahl, A., McAllister, M.R., Sansone, A., Dunlap, B.F., Desai, C., Wang, Y.-T., Balce, D.R., Luke, C.J., Lee, S., Orchard, R.C., et al. (2019). Autophagy genes in myeloid cells counteract IFN $\gamma$ -induced TNF-mediated cell death and fatal TNF-induced shock. *Proc. Natl. Acad. Sci. USA* **116**, 16497–16506.

Panchenko, M.V., Farber, H.W., and Korn, J.H. (2000). Induction of heme oxygenase-1 by hypoxia and free radicals in human dermal fibroblasts. *Am. J. Physiol. Cell Physiol.* **278**, C92–C101.

Patel, S.J., Sanjana, N.E., Kishton, R.J., Eidizadeh, A., Vodnala, S.K., Cam, M., Gartner, J.J., Jia, L., Steinberg, S.M., Yamamoto, T.N., et al. (2017). Identification of essential genes for cancer immunotherapy. *Nature* **548**, 537–542.

Perera, R.M., and Bardeesy, N. (2015). Pancreatic cancer metabolism: breaking it down to build it back up. *Cancer Discov.* **5**, 1247–1261.

Perera, R.M., Stoykova, S., Nicolay, B.N., Ross, K.N., Fitamant, J., Boukhali, M., Lengrand, J., Deshpande, V., Selig, M.K., Ferrone, C.R., et al. (2015). Transcriptional control of autophagy-lysosome function drives pancreatic cancer metabolism. *Nature* **524**, 361–365.

- Ryan, D.P., Hong, T.S., and Bardeesy, N. (2014). Pancreatic adenocarcinoma. *N. Engl. J. Med.* *371*, 1039–1049.
- Santana-Codina, N., Roeth, A.A., Zhang, Y., Yang, A., Mashadova, O., Asara, J.M., Wang, X., Bronson, R.T., Lyssiotis, C.A., Ying, H., and Kimmelman, A.C. (2018). Oncogenic KRAS supports pancreatic cancer through regulation of nucleotide synthesis. *Nat. Commun.* *9*, 4945.
- Sousa, C.M., Biancur, D.E., Wang, X., Halbrook, C.J., Sherman, M.H., Zhang, L., Kremer, D., Hwang, R.F., Witkiewicz, A.K., Ying, H., et al. (2016). Pancreatic stellate cells support tumour metabolism through autophagic alanine secretion. *Nature* *536*, 479–483.
- Sullivan, M.R., Danai, L.V., Lewis, C.A., Chan, S.H., Gui, D.Y., Kunchok, T., Dennstedt, E.A., Vander Heiden, M.G., and Muir, A. (2019). Quantification of microenvironmental metabolites in murine cancers reveals determinants of tumor nutrient availability. *eLife* *8*, e44235.
- Titov, D.V., Craican, V., Goodman, R.P., Peng, J., Grabarek, Z., and Mootha, V.K. (2016). Complementation of mitochondrial electron transport chain by manipulation of the NAD<sup>+</sup>/NADH ratio. *Science* *352*, 231–235.
- Towers, C.G., Fitzwalter, B.E., Regan, D., Goodspeed, A., Morgan, M.J., Liu, C.-W., Gustafson, D.L., and Thorburn, A. (2019). Cancer cells upregulate NRF2 signaling to adapt to autophagy inhibition. *Dev. Cell* *50*, 690–703.e6.
- Tsherniak, A., Vazquez, F., Montgomery, P.G., Weir, B.A., Kryukov, G., Cowley, G.S., Gill, S., Harrington, W.F., Pantel, S., Krill-Burger, J.M., et al. (2017). Defining a cancer dependency map. *Cell* *170*, 564–576.e16.
- Vande Voorde, J., Ackermann, T., Pfitzer, N., Sumpton, D., Mackay, G., Kalna, G., Nixon, C., Blyth, K., Gottlieb, E., and Tardito, S. (2019). Improving the metabolic fidelity of cancer models with a physiological cell culture medium. *Sci. Adv.* *5*, u7314.
- Vander Heiden, M.G., and DeBerardinis, R.J. (2017). Understanding the inter-connections between metabolism and cancer biology. *Cell* *168*, 657–669.
- Wang, X., and Lin, Y. (2008). Tumor necrosis factor and cancer, buddies or foes? *Acta Pharmacol. Sin.* *29*, 1275–1288.
- Wang, X., Wu, W.K.K., Gao, J., Li, Z., Dong, B., Lin, X., Li, Y., Li, Y., Gong, J., Qi, C., et al. (2019). Autophagy inhibition enhances PD-L1 expression in gastric cancer. *J. Exp. Clin. Cancer Res.* *38*, 140.
- Weiss, L., Hoffmann, G.E., Schreiber, R., Andres, H., Fuchs, E., Körber, E., and Kolb, H.J. (1986). Fatty-acid biosynthesis in man, a pathway of minor importance. Purification, optimal assay conditions, and organ distribution of fatty-acid synthase. *Biol. Chem. Hoppe Seyler* *367*, 905–912.
- Wu, J., and Lanier, L.L. (2003). Natural killer cells and cancer. *Adv. Cancer Res.* *90*, 127–156.
- Xu, R.H., Pelicano, H., Zhou, Y., Carew, J.S., Feng, L., Bhalla, K.N., Keating, M.J., and Huang, P. (2005). Inhibition of glycolysis in cancer cells: a novel strategy to overcome drug resistance associated with mitochondrial respiratory defect and hypoxia. *Cancer Res.* *65*, 613–621.
- Yamaguchi, N., Weinberg, E.M., Nguyen, A., Liberti, M.V., Goodarzi, H., Janjigian, Y.Y., Paty, P.B., Saltz, L.B., Kingham, T.P., Loo, J.M., et al. (2019). PCK1 and DHODH drive colorectal cancer liver metastatic colonization and hypoxic growth by promoting nucleotide synthesis. *eLife* *8*, e52135.
- Yamamoto, K., Venida, A., Yano, J., Biancur, D.E., Kakiuchi, M., Gupta, S., Sohn, A.S.W., Mukhopadhyay, S., Lin, E.Y., Parker, S.J., et al. (2020). Autophagy promotes immune evasion of pancreatic cancer by degrading MHC-I. *Nature* *581*, 100–105.
- Yang, S., Wang, X., Contino, G., Liesa, M., Sahin, E., Ying, H., Bause, A., Li, Y., Stommel, J.M., Dell'antonio, G., et al. (2011). Pancreatic cancers require autophagy for tumor growth. *Genes Dev.* *25*, 717–729.
- Yang, A., Rajeshkumar, N.V., Wang, X., Yabuuchi, S., Alexander, B.M., Chu, G.C., Von Hoff, D.D., Maitra, A., and Kimmelman, A.C. (2014). Autophagy is critical for pancreatic tumor growth and progression in tumors with p53 alterations. *Cancer Discov.* *4*, 905–913.
- Yang, A., Herter-Sprie, G., Zhang, H., Lin, E.Y., Biancur, D., Wang, X., Deng, J., Hai, J., Yang, S., Wong, K.-K., and Kimmelman, A.C. (2018). Autophagy sustains pancreatic cancer growth through both cell-autonomous and nonautonomous mechanisms. *Cancer Discov.* *8*, 276–287.
- Zhu, X.G., Nicholson Puthenveedu, S., Shen, Y., La, K., Ozlu, C., Wang, T., Klompstra, D., Gultekin, Y., Chi, J., Fidelin, J., et al. (2019). CHP1 regulates compartmentalized glycerolipid synthesis by activating GPAT4. *Mol. Cell* *74*, 45–58.e7.

## STAR★METHODS

### KEY RESOURCES TABLE

REAGENT or RESOURCE	SOURCE	IDENTIFIER
<b>Antibodies</b>		
HMBS	GeneTex	GTX113460; RRID: AB_10617763
GAPDH	Cell Signaling Technology	2118; RRID: AB_561053
HMOX1	Proteintech	10701-1-AP; RRID: AB_2118685
ATG7	Cell Signaling Technology	8558; RRID: AB_10831194
LC3B	Cell Signaling Technology	3868; RRID: AB_2137707
Caspase-8	Cell Signaling Technology	4790; RRID: AB_10545768
Cleaved caspase-8	Cell Signaling Technology	8592; RRID: AB_10891784
Caspase-3	Cell Signaling Technology	9665; RRID: AB_2069872
TNF-R1	Cell Signaling Technology	13377; RRID: AB_2798194
FLAG M2	Sigma-Aldrich	F1804; RRID: AB_262044
Anti-mouse H-2Kb/H-2Db	BioLegend	114602; RRID: AB_313593
PE anti-mouse H-2Kb/H-2Db	BioLegend	114607; RRID: AB_313598
Anti-mouse H-2Kb	Dr. Jon Yewdell	N/A
PE anti-human HLA-A,B,C	BioLegend	311405; RRID: AB_314874
PE anti-mouse PD-L1	BioLegend	124307; RRID: AB_2073557
RIP	Cell Signaling Technology	3493; RRID: AB_2305314
Phospho-RIP (Ser166)	Cell Signaling Technology	31122; RRID: AB_2799000
BUV395 Rat Anti-Mouse CD45	BD Biosciences	564279; RRID: AB_2651134
Brilliant Violet 605 anti-mouse CD8a	BioLegend	100744; RRID: AB_2562609
Brilliant Violet 711 anti-mouse CD3ε	BioLegend	100349; RRID: AB_2565841
Brilliant Violet 785 anti-mouse NK-1.1	BioLegend	108749; RRID: AB_2564304
Brilliant Violet 421 anti-mouse CD4	BioLegend	100438; RRID: AB_11203718
APC anti-mouse IFN-γ	BioLegend	505810; RRID: AB_315404
APC anti-mouse TNF-R1	BioLegend	113005; RRID: AB_2208780
Anti-mouse CD16/CD32	BioXCell	BE0307; RRID: AB_2736987
Peroxidase Goat Anti-Rabbit IgG (H+L)	Jackson ImmunoResearch Labs	111-035-144; RRID: AB_2307391
m-IgGκ BP-HRP	Santa Cruz	sc-516102; RRID: AB_2687626
Anti-Rabbit Secondary Antibody, Alexa Fluor 488	Thermo Fisher	A21206; RRID: AB_141708
<b>Bacterial and Virus Strains</b>		
NEB Stable Competent <i>E. coli</i>	NEB	C3040
<b>Chemicals, Peptides, and Recombinant Proteins</b>		
RPMI 1640	GIBCO	11875
DMEM	GIBCO	11965
Trypsin	GIBCO	25200
Penicillin-Streptomycin	GIBCO	15140122
FBS	Sigma	12306C
Phusion High-Fidelity PCR Master Mix with HF Buffer	NEB	M0531
BsmBI	NEB	R0580
T4 DNA Ligase	NEB	M0202
X-tremeGENE 9 DNA Transfection Reagent	Roche	6365779001
BamHI	NEB	R3136
NotI	NEB	R3189
Polybrene	Sigma	H9268
Puromycin	Sigma	P8833

(Continued on next page)

<b>Continued</b>		
REAGENT or RESOURCE	SOURCE	IDENTIFIER
Blasticidin	Invivogen	ant-bl
Matrigel Growth Factor Reduced	Corning	354230
MEM Amino Acids Solution (50X)	Thermo Fisher	11130
Normal donkey serum	Jackson ImmunoResearch	017-000-121
Recombinant Mouse IL-2	BioLegend	575404
Dynabeads Mouse T-Activator CD3/CD28	Thermo Fisher	11456D
Recombinant Mouse IFN- $\gamma$	BioLegend	575306
Recombinant Human IFN- $\gamma$	BioLegend	570206
APC Annexin V	BioLegend	640920
DAPI	Thermo Fisher	D1306
Zombie NIR Fixable Viability Dye	BioLegend	423106
Recombinant Mouse TNF- $\alpha$	BioLegend	575202
Recombinant Human TNF- $\alpha$	BioLegend	570104
Bafilomycin A1	Cayman Chemical	11038
Hemin	Sigma-Aldrich	H9039
Sodium pyruvate	Sigma-Aldrich	P2256
Necrostatin-1	Cayman Chemical	11658
Z-VAD-FMK	Selleckchem	S7023
ProLong Gold Antifade Mountant	Thermo Fisher	P36934
Fibronectin	Corning	54008
<b>Critical Commercial Assays</b>		
DNeasy Blood & Tissue Kit	QIAGEN	69506
Zyppy Plasmid Miniprep Kit	Zymo Research	D4019
Pierce BCA Protein Assay Kit	Thermo Fisher Scientific	23225
CD8a+ T Cell Isolation Kit, mouse	Miltenyi Biotec	130-104-075
RNeasy Mini Kit	QIAGEN	74104
<b>Deposited Data</b>		
RNaseq data	This Study	GEO: GSE158707
<b>Experimental Models: Cell Lines</b>		
KP panc	Dr. Nabeel M. Bardeesy	N/A
KP lung	Dr. Thales Papagiannakopoulos	N/A
AsPC-1	ATCC	N/A
MIA PACA-2	ATCC	N/A
PATU-8988T	ATCC	N/A
<b>Experimental Models: Organisms/Strains</b>		
Mouse: C57BL/6J	The Jackson Laboratory	000664
Mouse: B6.129S7-Rag1tm1Mom/J (Rag1 KO)	The Jackson Laboratory	002216
Mouse: C57BL/6-Tg(TcraTcrb)1100Mjb/J (OT-I)	The Jackson Laboratory	003831
Mouse: NOD.Cg-Prkdcscid Il2rgtm1Wjl/SzJ (NSG)	The Jackson Laboratory	005557
<b>Oligonucleotides</b>		
DNA oligonucleotides and primers	This Study	See <a href="#">Table S3</a>
<b>Recombinant DNA</b>		
CRISPR Cas9 sgRNA KO mouse metabolism library	This Study	N/A
CRISPR Cas9 sgRNA KO focused mouse metabolism library	This Study	N/A
pLenti CRISPR V2	Addgene	52961
pMXS-IRES-Blast	Cell Biolabs	RTV-016
pSECB	( <a href="#">Minton et al., 2018</a> )	N/A
pLenti CRISPR V2 sgmHmbs	This Study	N/A

(Continued on next page)

**Continued**

REAGENT or RESOURCE	SOURCE	IDENTIFIER
pSECB sgmHmox1	This Study	N/A
pLenti CRISPR V2 sgmAtg7	This Study	N/A
pLenti CRISPR V2 sgATG7	This Study	N/A
pLenti CRISPR V2 sgmRipk1	This Study	N/A
pLenti CRISPR V2 sgmTnfrsf1a	This Study	N/A
pLenti CRISPR V2 sgmTnfrsf1b	This Study	N/A
pLenti CRISPR V2 sgmHif1a	This Study	N/A
pLenti CRISPR V2 sgmEpas1	This Study	N/A
pLenti CRISPR V2 sgmTap1	This Study	N/A
pMXS-IRES-Blast mAtg7	This Study	N/A
pMP71-eGFP-OVA	This Study	N/A
pMP71-eGFP	This Study	N/A
pMXS-IRES-Blast cytoLbNOX	This Study	N/A
pMXS-IRES-Blast mitoLbNOX	This Study	N/A
pMXS-IRES-Blast mHmox1	This Study	N/A
pMXS-IRES-Blast mHmox1-H25A	This Study	N/A
Other		
Z2 Coulter Counter	Beckman	Model Z2
SpectraMax Microplate Reader	Molecular Devices	Model M3
Primovert Microscope	Carl Zeiss	415510-1105-000
REVOLVE4 Microscope	Echo Laboratories	FJSD1001

**RESOURCE AVAILABILITY****Lead Contact**

Further information and requests for resources and reagents should be directed to and will be fulfilled by the Lead Contact, Kıvanç Birsoy ([kbirsoy@rockefeller.edu](mailto:kbirsoy@rockefeller.edu)).

**Materials Availability**

CRISPR Cas9 sgRNA KO mouse metabolism library generated in this study has been deposited to Addgene (ID 160129). All other plasmids generated in this study can be requested from the Lead Contact.

**Data and Code Availability**

The RNaseq dataset generated in this study is available at GEO: GSE158707.

**EXPERIMENTAL MODEL AND SUBJECT DETAILS****Cell Culture**

The female mouse cell lines KP panc and KP lung were kindly provided by Dr. Nabeel M. Bardeesy (Massachusetts General Hospital Cancer Center) and Dr. Thales Papagiannakopoulos (New York University) respectively. Human cells lines AsPC-1, MIA-PaCa-2, PATU-8988T and HEK293T were purchased from the ATCC. Cell lines were verified to be free of mycoplasma contamination and the identities of all were authenticated by STR profiling. KP panc, KP lung and AsPC-1 cells were maintained in RPMI media (GIBCO) containing 2 mM glutamine, 10% fetal bovine serum, 1% penicillin and streptomycin. MIA PaCa-2, PATU-8988T and HEK293T cells were maintained in DMEM media (GIBCO) containing 4.5g/L glucose, 110mg/L pyruvate, 4mM glutamine, 10% fetal bovine serum, penicillin and streptomycin.

**Mouse Studies**

All animal studies and procedures were conducted according to a protocol approved by the Institutional Animal Care and Use Committee (IACUC) at the Rockefeller University. All mice were maintained on a standard light-dark cycle with food and water *ad libitum*. All treatment studies were randomized and injections were performed by blinded investigators. Subcutaneous tumor growth experiments were performed by injecting subcutaneously into the flanks of female 6-8-week-old C57BL/6J, Rag1 KO or NOD scid gamma (NSG) mice (The Jackson Laboratory), unless otherwise indicated at  $1-2 \times 10^6$  cells in 100  $\mu$ L 40% Matrigel (Corning). Mice were

sacrificed and tumors were dissected after 2-3 weeks. In no cases did any tumor size surpass the limit permitted by our protocol (2 cm). The immune-dependent difference we observed is not due to rejection by mice of the opposite gender as almost identical results were obtained in C57BL/6J mice of both genders (Figure S3C). For orthotopic pancreas injections, mice were anaesthetized by an intraperitoneal injection of ketamine. A small incision was made on the upper left quadrant of the abdomen and the pancreas was externalized. Cells were suspended in 50  $\mu$ L of Matrigel: PBS (1:1) solution and injected into the pancreatic tail with insulin syringes (29-gauge needle, BD). Approximately  $1 \times 10^5$  KP panc cells were injected and after the procedures, the peritoneum was closed with a 3-0 Vicryl Violet suture (Ethicon), and the skin was closed using the BD AutoClip Wound Closing System (BD). Mice were sacrificed and tumors were dissected after 2 weeks.

## METHOD DETAILS

### CRISPR-based Screens

The metabolism and focused sgRNA libraries were designed and screens were performed as previously described (Garcia-Bermudez et al., 2019; Zhu et al., 2019). Focused sgRNA screens for KP panc and KP lung cell lines in C57BL/6J and NSG mice were carried out together. Oligonucleotides for sgRNAs were synthesized by CustomArray and amplified by PCR. For *in vivo* screens, library infected cells were injected subcutaneously into the flanks of 6-8-week-old C57BL/6J or NOD scid gamma (NSG) mice (The Jackson Laboratory) at  $1 \times 10^6$  cells in 100  $\mu$ L 40% Matrigel. Tumors were grown for 2-3 weeks and gDNAs were extracted with DNeasy Blood & Tissue Kit (QIAGEN). gDNAs from 4 tumors were pooled as one sample and amplified by PCR. PCR amplicons were then sequenced together with the initial and *in vitro* samples as per standard *in vitro* CRISPR-based screens. We then performed PCA analysis on normalized counts from each mouse, as well as the initial and *in vitro* samples. Based on this outlier analysis, one of the mice was filtered from the downstream analysis. Sequencing counts from *in vivo* tumor samples were then summed, normalized (count per million), and analyzed as a single condition. The fitness score for each guide was calculated as  $\log_2$  ratio of normalized counts. The median of the guides was used as the fitness score for each gene, and t test was used to assess whether the guides were significantly deviating from 0. For iPAGE analysis of fitness scores between *in vivo* and *in vitro* screens, the differential scores across all genes were used as input to iPAGE with the following parameters: ebins = 3, max\_p = 0.05, and using MSigDB c2 gene sets. A complete list of differential gene scores for each screen is provided in Table S1.

### Immunoblot

Cell pellets were washed twice with ice-cold PBS prior to lysis in RIPA buffer (10 mM Tris-Cl pH 7.5, 150 mM NaCl, 1 mM EDTA, 1% Triton X-100, 0.1% SDS) supplemented with protease inhibitors and phosphatase inhibitors (Roche). For tumor tissue samples, 50 mg tissues were taken from each sample and homogenized in RIPA buffer by Bead Ruptor 24 (Omni International). Each lysate was sonicated and, after centrifugation for 5 min at 4°C and 20,000 x g, supernatants were collected. Sample protein concentrations were determined by using Pierce BCA Protein Assay Kit (Thermo Scientific) with bovine serum albumin as a protein standard. Samples were resolved on 12% or 10%–20% SDS-PAGE gels and analyzed by immunoblotting as previously described (Birsoy et al., 2014).

### Generation of Knock-out and cDNA Overexpression Cell Lines

sgRNAs (oligonucleotide sequences are indicated in Table S3) were cloned into lentiCRISPR-v2 linearized with BsmBI by T4 ligase (NEB). sgRNA expressing vector along with lentiviral packaging vectors Delta-VPR and CMV VSV-G were transfected into HEK293T cells using the XTremeGene 9 transfection reagent (Roche). Similarly, for overexpression cell lines, gBlocks (IDT) containing the cDNA of interest were cloned into pMXS linearized with BamHI and NotI by Gibson Assembly (NEB). cDNA vectors along with retroviral packaging vectors gag-pol and CMV VSV-G were transfected into HEK293T cells. The virus-containing supernatant was collected 48 h after transfection and passed through a 0.22  $\mu$ m filter to eliminate cells. Target cells in 6-well tissue culture plates were infected in media containing 8  $\mu$ g/mL of polybrene and a spin infection was performed by centrifugation at 2,200 rpm for 1 h. Post-infection, virus was removed and cells were selected with puromycin or blasticidin. For Atg7 knockout cells, after selection, cells were single-cell diluted into the wells of a 96-well plate. Cells were grown for two weeks, and the resultant colonies were expanded. Clones were validated for loss of the relevant protein via immunoblotting.

### Cell Proliferation and Survival Assays

For cell proliferation assays with KP panc and KP lung cells, cells were plated in triplicates in 6-well plates at 10000 cells/well. Cells were dissociated with trypsin at the indicated days and counted by Z2 Coulter Counter (Beckman). 300000 cells/well were then plated in new plates and counted again at the indicated days. For survival assays with chemical treatments, cells were plated in triplicates in 12-well plates and allowed to adhere for 2 h before adding chemicals. Chemicals were added on the day of plating unless otherwise indicated. Cells were plated at 200000 cells/well and counted after 2 days or plated at 100000 cells/well and counted after 3 days.

### Patient-Derived Pancreatic Cancer Xenografts

PDX model was described previously (Yamaguchi et al., 2019). Low passage PDX pancreatic tumor was chopped finely with a scalpel and placed in a 50 mL conical tube with a solution of Dulbecco's Modified Eagle Medium (GIBCO) supplemented with 10% v/v fetal

bovine serum (Corning), L-glutamine (2 mM; GIBCO), penicillin-streptomycin (100 U/mL; GIBCO), Amphotericin (1  $\mu$ g/mL; Lonza), sodium pyruvate (1 mM; GIBCO) and Collagenase, Type IV (200 U/mL; Worthington) and placed in a 37°C shaker at 220 rpm for 30 min. After centrifugation and removal of supernatant, the sample was subjected to ACK lysis buffer (Lonza) for 3 min at room temperature to remove red blood cells. After centrifugation and removal of ACK lysis buffer, the sample was subjected to a density gradient with Optiprep (1114542, Axis-Shield) to remove dead cells. The sample was washed in media and subjected to a 100- $\mu$ m cell strainer and followed by a 70- $\mu$ m cell strainer. Mouse cells were removed from the single-cell suspension via magnetic-associated cell sorting using the Mouse Cell Depletion Kit ((130-104-694, Miltenyi), resulting in a single-cell suspension of predominantly pancreatic cancer cells of human origin. 10 million PDX pancreatic cancer cells were transduced with the indicated sgRNA library and washed with PBS. Cells were resuspended in cold PBS with 50% Matrigel and one million cells were injected subcutaneously into NSG mice. When the tumors reached palpable size (70 mm<sup>3</sup>), mouse was euthanized and the tumors were removed and sectioned in a manner similar to the *in vivo* CRISPR-based screens.

### Immunohistochemistry

Tumor samples were removed from mice at the time of sacrifice and fixed in 10% buffered formalin for 48 h. Samples were maintained in 70% ethanol. Fixed tumor samples were then embedded in paraffin, sectioned and stained with the indicated antibodies.

### Immune Profiling of Tumors

Tumors were excised and digested for 1 h at 37°C with 400U/mL of collagenase D (Roche). Hematopoietic cells enrichment was achieved by density gradient centrifugation with 40/90 Percoll (GE Healthcare Life Sciences) for 25 min at 2500rpm at 22°C with zero breaks. Interphase containing the hematopoietic cells was isolated and washed with PBE. Red cell lysis was performed with ACK lysis buffer (GIBCO). For cytokine staining, cells were incubated at 37°C for 4 h in complete RPMI media supplemented with Brefeldin A (Sigma), phorbol 12-myristate 13-acetate (PMA) (Sigma) and Ionomycin (Sigma). After incubation cells were washed with PBE. Cells were incubated for 5 min with 1ug/mL of anti-CD16/32 (2.4G2, BioXcell) at room temperature. Cells were washed with PBS and stained with Zombie fixable viability dye (Biolegend) for 15 min at room temperature. Cells were washed with PBE and stained with appropriate surface markers antibodies for CD4 and CD8 T cells and NK cells for 20 min at 4°C. Cells were washed with PBE fixed and permeabilized with Cytotfix/Cytoperm kit (BD). Intercellular staining for IFN $\gamma$  and TNF $\alpha$  was performed for 30 min at 4°C. Cells were washed and resuspended in PBE. Samples were acquired on the BD FACSymphony. Data were analyzed using FlowJo v.10.0.8 software.

### OT-I T Cell Co-culture

OT-I T cells were isolated from OT-I transgenic mice (The Jackson Laboratory) by extracting cells from lymph nodes using the CD8a<sup>+</sup> T Cell Isolation Kit (Miltenyi Biotec) and following manufacturer's instructions. T cells were cultured in T cell media (RPMI media (GIBCO) containing 2 mM glutamine, 10% fetal bovine serum, 1% penicillin and streptomycin, 1 mM pyruvate, 50  $\mu$ M 2-mercaptoethanol and 1X MEM Amino Acids Solution (GIBCO) with 20 ng/mL IL-2). T cells were activated by Dynabeads Mouse T-Activator CD3/CD28 (Thermo Fisher Scientific) and allowed to proliferate for 6 days. One day prior to co-culture, KP panc cancer cells were seeded in 12-well plates at 50000 or 100000 cells/well with 100 ng/mL IFN $\gamma$ . The following day, each well with cancer cells was changed to 500  $\mu$ L fresh media. Activated CD8<sup>+</sup> T cells were resuspended in the indicated E:T ratios and added to each well in 500  $\mu$ L T cell media. After 48 h, T cells were washed off and cancer cells were counted. For flow cytometry of apoptotic cells, cancer cells were dissociated and washed with PBS. Cells were stained for 15 min at room temperature in the dark with APC Annexin V (BioLegend) and resuspended in PBS with DAPI. Cells were analyzed on a LSRFortessa (BD Biosciences).

### Flow Cytometry

For staining of MHC-I, cells were treated for 24 h with the indicated concentration of IFN $\gamma$  and one million cells were resuspended in PBS supplemented with 0.5% BSA and 2mM EDTA (PBE). Cells were incubated for 5 min with 1ug/mL of anti-CD16/32 (2.4G2, BioXcell) at room temperature. Cells were washed with PBS and stained with Zombie fixable viability dye (Biolegend) 15 min at room temperature. Cells were washed with PBE and stained with PE anti-mouse H-2Kb/H-2Db or PE anti-human HLA-A,B,C (Biolegend) antibody for 20 min at 4°C. Cells were washed and resuspended in PBE. Samples were acquired on the BD FACSymphony. Data were analyzed using FlowJo v.10.0.8 software.

For staining of TNFR1, one million cells were resuspended in PBS supplemented with 1% BSA and 1mM EDTA (FACS buffer). Cells were washed with FACS buffer and stained with APC anti-mouse TNFR1 (Biolegend) antibody for 15 min at 4°C in the dark. Cells were washed and resuspended in FACS buffer with 60 ng/mL DAPI. Samples were acquired on the BD FACSymphony. Data were analyzed using FlowJo v.10.0.8 software.

### RNaseq

For *in vitro* samples, cells were cultured as indicated and RNA was extracted using RNeasy mini kit (QIAGEN) following manufacturer's protocol. For tumor samples, tumors were dissected 2 weeks after injection. A 20 mg tissue from each sample was homogenized using Bead Ruptor 24 (Omni International) and RNA was processed using RNeasy mini kit following manufacturer's protocol. Purified total RNA was cleaned up and mRNA was sequenced by NextSeq High Output. For analysis, reads were mapped to the mouse transcriptome (mm10, Ensembl annotations) using STAR (v2.7). FeatureCounts (v1.6) was used to count exonic reads

(with -O option) and DESeq2 v1.20 (R v3.5.1) was used to normalize and compare samples. PCA plots were generated using the plotPCA function (DESeq2) after variance stabilization and dispersion estimation. Log-fold changes across all genes were used as input to iPAGE with the following parameters: ebins = 9, max\_p = 0.005, and using MSigDB h gene sets (i.e., the Hallmarks gene set collection).

### Survival Analysis

TCGA-PAAD gene expression data (FPKM, downloaded from Genomic Data Commons on 10/13/2016) and the associated clinical data (cBioportal) were used to perform survival analysis. For gene signatures, the expression of each gene was first z-score normalized and the signature score was calculated as the weighted sum of the z-scores. Given the short survival of PAAD patients, the analysis was limited to 3 years. To determine the separation threshold, the samples were divided based on their signature score or expression levels at every value between the 10<sup>th</sup> and 90<sup>th</sup> percentiles. Survival analysis was then performed using the survdiff function (survival package in R) and the value with the lowest *p*-value was selected as the threshold. The function survfit was then used to perform the analysis at that threshold and visualize the Kaplan-Meier plot.

### Immunofluorescence

For immunofluorescence assays in glass-bottom 8-well slides, cells were seeded at 7500 cells per well after pretreating the glass with fibronectin. 24 h later, cells were treated with 70 ng/mL IFN $\gamma$ . After 22 h, cells were stained with anti-H-2Kb/H-2Db antibody (1:200, Biolegend) for 2 h at 37°C before fixing with 4% paraformaldehyde in PBS for 10 min at room temperature. After three washes with PBS, cells on coverslips were permeabilized and blocked by incubation with 0.2% Triton-X in PBS + 5% normal donkey serum (NDS) for 1 h at room temperature, shaking. Cells on coverslips were subsequently incubated with anti-H-2Kb/H-2Db 1:200 for 16 h at 4°C before washing 3 times with PBS. Coverslips were then incubated with secondary (Alexa Fluor 568 anti-mouse) 1:500 in 5% NDS + 0.2% Triton in PBS for 1 h and washed 3 times with PBS. Finally, coverslips were mounted onto slides with Prolong Gold Antifade mounting media (Invitrogen).

Confocal images were acquired with a Zeiss inverted LSM 780 laser scanning confocal microscope (Zeiss) using a 63x/1.4 DIC Plan-Apochromat oil immersion objective. Images were obtained with excitation and emission wavelengths as follows: DAPI 405-464, Alexa Fluor 568 561-605. The images are 1192 × 1192 pixels with a pixel depth of 16-bit, with a pixel size of 14.0204 $\mu$ m per pixel, a dwell time of 1.58 $\mu$ s, a pinhole size of 11.2 (1Airy unit), and a line averaging of 1.

### QUANTIFICATION AND STATISTICAL ANALYSIS

Sample size, mean, and significance *p* values are indicated in the text and figure legends. Error bars in the experiments represent standard deviation (SD) from either independent experiments or independent samples. Student's *t* test was used for comparisons with single variable. ANOVA was used for comparisons with two or more variables. Statistical analyses were performed using GraphPad Prism 7 or reported by the relevant computational tools.